JOURNAL OF MOLECULAR SPECTROSCOPY **192,** 152–161 (1998)
ARTICLE NO. MS987633

Infrared and Microwave Spectra and Force Field of DBO: The Coriolis Interaction between the ν_1 and $\nu_2 + \nu_3$ States

Yoshiyuki Kawashima,* Pina Colarusso,† K. Q. Zhang,† Peter Bernath,† and Eizi Hirota‡

*Department of Applied Chemistry, Kanagawa Institute of Technology, 1030 Shimo-ogino, Atsugi, Kanagawa 243-0203, Japan; †Department of Chemistry, University of Waterloo, Waterloo, Ontario, Canada N2L 3G1; and ‡The Graduate University for Advanced Studies, Hayama, Kanagawa 240-0193, Japan

Received March 25, 1998

The ν_1 and ν_3 bands of $D^{11}BO$ and the ν_1 band of $D^{10}BO$ were observed by using an infrared diode laser spectrometer. The DBO molecule was generated by an ac discharge in a mixture of BCl_3, D_2, O_2, and He. As inferred previously, a strong Coriolis interaction was in fact found to take place between the ν_1 and $\nu_2 + \nu_3$ states, and an analysis of the observed ν_1 spectra, which explicitly took into account this Coriolis interaction, predicted the pure rotational transition frequencies of DBO in the ν_1 state. Pure rotational lines were then detected by microwave spectroscopy, confirming the validity of the infrared assignment. In the microwave experiment DBO molecules were generated by a discharge in a mixture of B_2D_6 and O_2. The three fundamental bands and a hot band of $D^{11}BO$, as well as the ν_1 and ν_3 bands of $D^{10}BO$, were subsequently recorded in emission with a Fourier transform infrared spectrometer. DBO molecules were generated by the reaction of D_2 with HBO at temperatures above 800°C in a ceramic tube furnace. All of the observed spectra were simultaneously subjected to a least-squares analysis to obtain molecular parameters in the ground, ν_1, ν_2, ν_3, and $\nu_2 + \nu_3$ states. The results thus obtained improved the force field and molecular structure of the HBO/DBO molecules reported in a previous study (Y. Kawashima, Y. Endo, and E. Hirota, 1989, *J. Mol. Spectrosc.* **133,** 116–127). © 1998 Academic Press

I. INTRODUCTION

The transient molecule HBO is linear and isoelectronic with HCN, and it is quite interesting to compare the properties of the two species. HBO and its derivatives, such as *X*BO, with *X* denoting a halogen atom, seem to be much more reactive than their sulfur analogues; the parent molecule of the sulfur series HBS was studied by microwave spectroscopy in as early as 1973 (*1*), whereas the detection of HBO was not possible until 1986. Kawashima *et al.* succeeded in observing the ν_3 band of HBO by using a discharge-modulated infrared diode laser spectrometer (*2*), and the rotational spectra were measured not only in the ground vibrational state but also in the ν_1, ν_2, $2\nu_2$, and ν_3 excited states with a millimeter-wave spectrometer (*3*). They extended the microwave observations to several isotopic species in order to determine the equilibrium molecular structure as well as the harmonic and the third-order anharmonic force constants (*4*). It should be noted, however, that although the rotational transitions in the ν_1 state were observed clearly for HBO (*3*), it was not possible to detect them for DBO. Kawashima *et al.* (*4*) ascribed this failure to observe the ν_1 satellites for DBO to the Coriolis interaction between the ν_1 and $\nu_2 + \nu_3$ states; the energy difference between the two states was estimated to be about 200 cm^{-1} for HBO, but to be as small as 10 cm^{-1} in DBO.

In the present study we have extended the infrared observations with a particular focus on the detection of the ν_1 band of DBO. We have supplemented the infrared measurements by observing the ν_1 satellite lines by microwave spectroscopy. Recently the infrared emission spectra of HBO and DBO were recorded in the region from 350 to 3600 cm^{-1} using a Fourier transform infrared spectrometer at a resolution of 0.01 cm^{-1} (*5*). We have completed the simultaneous analysis of all of the observed spectra of DBO by explicitly taking into account the effects of the Coriolis interaction.

II. EXPERIMENTAL DETAILS

The infrared diode laser spectrometer used was the same as that reported earlier (*6, 7*). The glow discharge cell employed was made of a 1-m-long glass tube 65 mm in inner diameter. The effective path length was chosen to be about 10 m using a White-type multiple reflection configuration. DBO molecules were produced by an ac discharge in a mixture of BCl_3, D_2, O_2, and He. The optimal conditions for the production of DBO were attained when the partial pressures of BCl_3, D_2, and He were 60, 120, and 4000 mTorr, respectively, and when a trace of O_2 was added to this mixture. Source frequency modulation was employed instead of discharge modulation because neither precursors nor products absorbed strongly in the frequency region scanned. The observed wavenumbers were calibrated using the N_2O ν_1 band, the CO_2 ν_3 band, and the CO fundamental band in the 2250 cm^{-1} region (*8*) and the NH_3 ν_4 band in the 1600 cm^{-1} region (*9*) as wavelength standards, and a vacuum-spaced étalon was used as an interpolation device. The spectrum of $D^{10}BO$ was observed in natural abundance.

The source–frequency modulation microwave spectrometer employed was described in detail in Refs. (*10, 11*). The reac-

0022-2852/98 $25.00

tion of BCl_3 with a mixture of H_2 and O_2 yielded a spectral intensity of HBO approximately one-third as large as the reaction of B_2H_6 with O_2 and thus could not be employed to observe weak rotational transitions in the excited vibrational states lying as high as 2000 cm^{-1}. Therefore, DBO molecules were generated by an ac discharge in a B_2D_6 and O_2 mixture directly inside a free space absorption cell which was 100 mm in diameter and 1 m in length. The observed spectral intensity reached a peak when the partial pressures of B_2D_6 and O_2 were 10 and 20 mTorr, respectively, and the discharge current was 40–50 mA.

In the Fourier-transform infrared emission experiments carried out at the University of Waterloo, DBO was generated in a high-temperature reaction of HBO with D_2 gas. The parent molecule HBO was produced by heating boron in a ceramic tube furnace; the chemistry of the HBO formation is described in more detail in a separate report (*12*). Two tantalum boats containing 10 g of amorphous boron were placed near the middle of a mullite ($3Al_2O_3 \cdot 2SiO_2$) tube. The tube was sealed with KRS-5 windows at both ends and evacuated through a pumping port.

The central 50-cm portion of the tube was housed in a high-temperature furnace (CM Rapid-Temp) and was heated at a rate of 5°C/min up to 1200°C. A Ge-coated KBr beam splitter was used for all the runs. To reduce the contamination from atmospheric water and carbon dioxide, the region between the tube and the spectrometer was purged with dry nitrogen.

Once the infrared emission from HBO was observed (starting at 830–850°C), deuterium was introduced into the tube furnace through a gas inlet. A slow pumping speed was maintained throughout the experiment. DBO spectra were recorded at a resolution of 0.01 cm^{-1} from 350 to 700 cm^{-1} with a liquid-helium-cooled Si:B detector and from 1400 to 2600 cm^{-1} with a liquid-nitrogen-cooled HgCdTe (MCT) detector. The wavenumber range measured by the detectors was narrowed with appropriate bandpass and redpass filters. Each spectrum corresponds to a Fourier transform of 40 coadded interferograms. The spectra were calibrated using vibrational–rotational (*13*) and pure rotational lines (*14*) of HCl, which was present as an impurity.

Details of the DBO emission spectra are given in Figs. 1–3 for the ν_1, ν_2, and ν_3 bands, respectively. Both of the naturally abundant boron isotopomers (^{11}B 80.1% and ^{10}B 19.9%) were detected. All three fundamental bands as well as several hot bands were assigned for the major isotopomer $D^{11}BO$, and two of the three fundamental bands were observed for the minor $D^{10}BO$ species.

III. SPECTRAL ANALYSIS AND RESULTS

Lory and Porter (*15*) reported the ν_1 fundamental band of $D^{11}BO$ in a low-temperature matrix to be at 2259 cm^{-1}. By referring to this value, the region from 2220 to 2300 cm^{-1} was scanned by using the infrared diode laser spectrometer, and 13 lines were observed. Although these lines exhibited a pattern

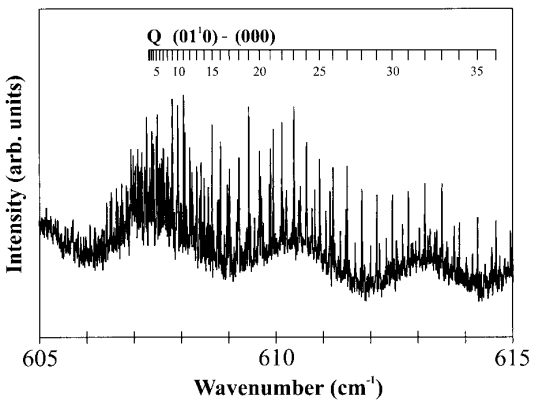

FIG. 1. A detail of the Fourier transform infrared emission spectrum of DBO in the fundamental bending region. A portion of the *Q* branch is labeled for the (01^10)–(000) transition of the $D^{11}BO$ isotopomer. The spectrum was recorded with a liquid-helium-cooled Si:B detector at a resolution of 0.01 cm^{-1}.

close to a parallel band of a linear molecule, they did not fit the predicted pattern exactly. This observation indicated that the ν_1 state is perturbed by another vibrational state, possibly by the $\nu_2 + \nu_3$ state, as presumed in a previous study (*4*), and as suggested by the energy diagram of DBO shown in Fig. 4. Therefore, the observed spectra were analyzed by including effective Coriolis interaction Hamiltonian matrix elements of the following form,

$$\langle v_s + 1,\, v_t - 1,\, l,\, J|\mathbf{H}_{\mathrm{cor}}|v_s,\, v_t,\, l \pm 1,\, J\rangle = B_e\zeta_{st}^{\mathrm{eff}}[(\omega_t/\omega_s)^{1/2} + (\omega_s/\omega_t)^{1/2}][(v_s + 1) \times (v_t \pm l + 1)]^{1/2}[(J \mp l)(J \pm l + 1)]^{1/2}/2,$$

where B_e denotes the equilibrium rotational constant, $\zeta_{st}^{\mathrm{eff}}$ the effective Coriolis coupling constant between the nondegenerate s (ν_1) and degenerate t ($\nu_2 + \nu_3$) states, and ω_s and ω_t represent the vibrational energies of the two states, respectively. We employed this general expression by setting $v_s = 0$, $v_t = 1$, and $l = 0$, namely the matrix element equal to

$$\langle v_s = 1,\, v_t = 0,\, l = 0,\, J|\mathbf{H}_{\mathrm{cor}}|v_s = 0,\, v_t = 1,\, l = \pm 1,\, J\rangle = B_e\zeta_{st}^{\mathrm{eff}}[(\omega_t/\omega_s)^{1/2} + (\omega_s/\omega_t)^{1/2}][J(J + 1)/2]^{1/2}.$$

The adjusted parameters were chosen to be the band origin ν_1, the rotational constant B_1 of the ν_1 state, the effective Coriolis coupling constant, and the energy difference between the ν_1 and $\nu_2 + \nu_3$ states. The ground state parameters and rotational and centrifugal distortion constants were fixed to the previously reported values (*4*), and rotational and centrifugal distortion and *l*-type doubling constants of the $\nu_2 + \nu_3$ state were estimated from the constants of the ν_2 and ν_3 fundamental states.

We then checked the assignment of the infrared spectra by observing rotational transitions. The infrared results predicted

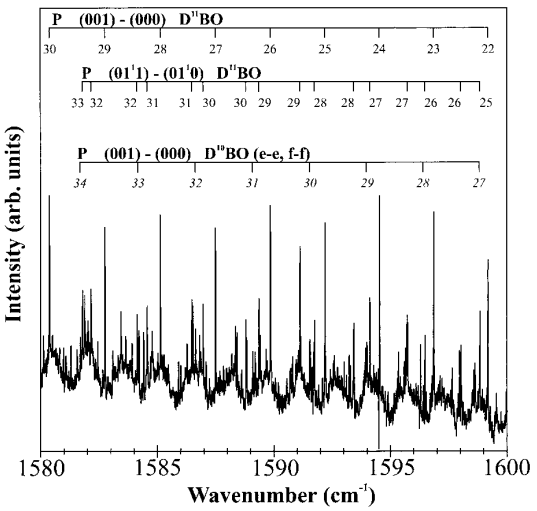

FIG. 2. A detail of the Fourier transform infrared emission spectrum of DBO. *P*-branch lines arising from the (001)–(000) fundamental transition are shown for both $D^{11}BO$ and $D^{10}BO$. *P*-branch lines for the (01^11)–(01^10) vibrational band of $D^{11}BO$ are also indicated. The spectrum was recorded with a liquid-nitrogen-cooled HgCdTe detector at a resolution of 0.01 cm^{-1}.

the $J = 6 \leftarrow 5$ and $J = 3 \leftarrow 2$ transitions of $D^{11}BO$ in the ν_1 state to appear at 372 865 and 186 423 MHz, respectively, and they were in fact observed at 372 865.852 and 186 422.644 MHz, respectively. The observed lines are listed in Table 1 with their assignments.

A number of absorption lines remained in the region from 2220 to 2300 cm^{-1} and most of them were assigned to the ν_1 band of $D^{10}BO$. We again found for this species that five *P*-branch transitions could not be fitted unless we took into account the Coriolis interaction of ν_1 with $\nu_2 + \nu_3$. The infrared diode laser observations were extended to the region from 1610 to 1630 cm^{-1}, where four lines were observed and assigned to the ν_3 band of $D^{11}BO$.

Subsequently the ν_1, ν_2, ν_3, and $\nu_2 + \nu_3 - \nu_2$ bands of $D^{11}BO$ and the ν_1 band of $D^{10}BO$ were observed in emission using the Fourier-transform infrared spectrometer (*5*). The spectral lines thus observed were assigned based upon the infrared diode laser and microwave results. The emission measurements extended the infrared data set to high *J*, to approximately 400 rotational–vibrational lines.

All of the infrared and microwave transitions observed for $D^{11}BO$ are listed in Table 1 with the assignments. We analyzed all of the observed data simultaneously by the least-squares method. The microwave transitions were weighted 10^5–10^6 more than the infrared transitions in accordance with the precision of each measurement. The adjusted parameters included vibrational frequencies, rotational and centrifugal distortion constants, *l*-type doubling constants of the ground, ν_1, ν_2, ν_3, and $\nu_2 + \nu_3$ states, and the effective Coriolis coupling constant. As shown in Table 2, the present results are in good agreement with the microwave data previously reported in (*4*), whenever a comparison is possible.

Table 3 summarizes the spectroscopic data obtained so far for the less abundant isotopic species $D^{10}BO$. The ν_1 band of this species was analyzed in a way similar to the case for $D^{11}BO$, but because the observed data were limited, only the band origin ν_1, rotational and centrifugal distortion constants of the ground and ν_1 states, and the effective Coriolis coupling constant were chosen as adjustable parameters. Table 2 shows that the vibrational frequency observed for the $\nu_2 + \nu_3$ state of $D^{11}BO$, 2262.96084 (81) cm^{-1}, is higher by 6.9 cm^{-1} than the sum of the ν_2 and ν_3 fundamental states, 2256.05232 cm^{-1}. This shift of the vibrational frequency obtained for $D^{11}BO$ was transferred to the $\nu_2 + \nu_3$ state of $D^{10}BO$, where the ν_2 frequency was as-

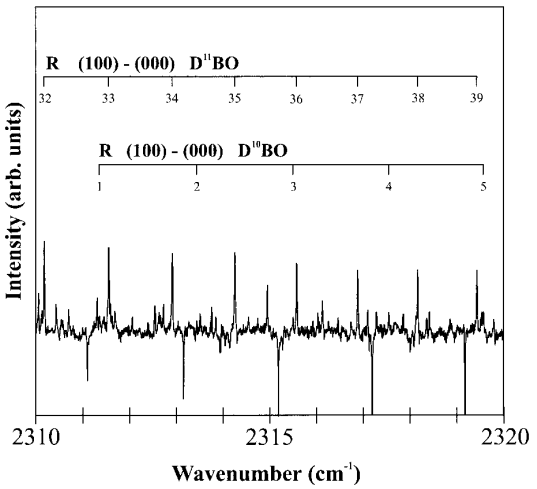

FIG. 3. A portion of the Fourier transform infrared emission spectrum of $D^{11}BO$. *R*-branch lines in the (100)–(000) vibrational band are labeled for both $D^{11}BO$ and $D^{10}BO$. The spectrum was obtained with a liquid-nitrogen-cooled HgCdTe detector at a resolution of 0.01 cm^{-1}.

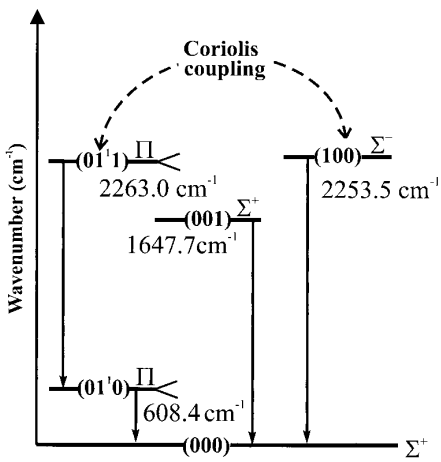

FIG. 4. The infrared transitions of DBO that were observed in emission. A Coriolis interaction occurs between the (01^10) and (100) vibrational energy levels. The analysis presented here includes vibrational–rotational as well as pure rotational transitions.

TABLE 1

Rotational–Vibrational and Pure Rotational Line Positions for $D^{11}BO$[a,b]

J'	J''	*Obs.*	O-C	J'	J''	*Obs.*	O-C	J'	J''	*Obs.*	O-C
						(100)—(000)					
52	53	2114.8500	-0.0004	17	18	2212.1987	-0.0001	19	18	2288.8963	0.0002
51	52	2117.8993	0.0001	16	17	2214.6763	0.0004	20	19	2290.5425	0.0005
50	51	2120.9320	-0.0009	15	16	2217.1338	-0.0001	21	20	2292.1656	-0.0027
49	50	2123.9529	0.0014	14	15	2219.5724	0.0001	22	21	2293.7749	0.0001
48	49	2126.9546	-0.0003	13	14	2221.9916	0.0008	23	22	2295.3637	0.0016
47	48	2129.9429	-0.0002	12	13	2224.3883	-0.0006	24	23	2296.9297	-0.0002
46	47	2132.9139	-0.0021	11	12	2226.7663	0.0000	25	24	2298.4794	0.0009
45	46	2135.8738	0.0001	10	11	2229.1226	0.0000	26	25	2300.0078	-0.0002
44	45	2138.8168	0.0008	9	10	2231.4583	0.0010	27	26	2301.5186	0.0002
43	44	2141.7466	0.0037	8	9	2233.7697	-0.0002	28	27	2303.0098	0.0000
42	43	2144.6541	-0.0003	7	8	2236.0604	0.0003	29	28	2304.4821	-0.0002
41	42	2147.5500	-0.0004	6	7	2238.3273	-0.0002	30	29	2305.9360	0.0001
40	41	2150.4310	0.0003	5	6	2240.5721	0.0006	31	30	2307.3699	-0.0006
39	40	2153.2954	-0.0002	4	5	2242.7929	0.0012	32	31	2308.7865	0.0002
38	39	2156.1441	-0.0006	3	4	2244.9860	-0.0021	33	32	2310.1838	0.0005
37	38	2158.9781	0.0000	2	3	2247.1607	0.0007	34	33	2311.5614	-0.0001
36	37	2161.7954	-0.0003	1	2	2249.3066	-0.0007	35	34	2312.9205	-0.0002
35	36	2164.5974	-0.0001					36	35	2314.2601	-0.0011
34	35	2167.3854	0.0020	0	1	2251.4306	0.0007	37	36	2315.5829	0.0000
33	34	2170.1510	-0.0021	1	0	2255.5969	-0.0034	38	37	2316.8846	-0.0010
32	33	2172.9058	-0.0011	3	2	2259.6681	-0.0031	39	38	2318.1700	0.0004
31	32	2175.6449	0.0005	5	4	2263.6452	0.0015	40	39	2319.4335	-0.0011
30	31	2178.3644	-0.0012	6	5	2265.5942	0.0006	41	40	2320.6815	0.0009
29	30	2181.0700	-0.0005	7	6	2267.5197	0.0001	42	41	2321.9084	0.0006
28	29	2183.7590	0.0002	8	7	2269.4224	0.0003	43	42	2323.1161	0.0000
27	28	2186.4302	-0.0005	9	8	2271.3012	-0.0003	44	43	2324.3053	0.0000
26	27	2189.0861	0.0004	10	9	2273.1582	0.0001	45	44	2325.4746	-0.0009
25	26	2191.7241	0.0003	11	10	2274.9928	0.0006	46	45	2326.6279	0.0013
24	25	2194.3450	0.0001	12	11	2276.8027	-0.0015	47	46	2327.7565	-0.0021
23	24	2196.9484	-0.0003	13	12	2278.5997*	0.0052	48	47	2328.8728	0.0012
22	23	2199.5352	0.0000	14	13	2280.3644	0.0011	49	48	2329.9645	-0.0009
21	22	2202.1050	0.0009	15	14	2282.1115	0.0005	50	49	2331.0430	0.0030
20	21	2204.6553	0.0003	16	15	2283.8392	0.0013	51	50	2332.0950	-0.0004
19	20	2207.1879	-0.0001	17	16	2285.5442	-0.0001	52	51	2333.1304	-0.0011
18	19	2209.7033	0.0006	18	17	2287.2315	0.0012				
						(01^10)—(000), e—e					
35	36	533.0650	-0.0003	8	9	588.4929	-0.0002	21	20	651.6587	-0.0001
34	35	535.0876	0.0009	7	8	590.5761	-0.0005	22	21	653.7801	-0.0005
33	34	537.1114	0.0006	5	6	594.7481	-0.0013	23	22	655.9033	0.0005
32	33	539.1373	0.0000	4	5	596.8396	0.0011	24	23	658.0263	0.0007
31	32	541.1640	-0.0025	3	4	598.9319	0.0025	25	24	660.1493	0.0005
30	31	543.1996	0.0014	2	3	601.0222	0.0001	26	25	662.2726	0.0003
29	30	545.2319	-0.0005	1	2	603.1093	-0.0072	27	26	664.3965	0.0004
28	29	547.2665	-0.0027	2	1	611.5066	-0.0037	28	27	666.5208	0.0007
27	28	549.3080	-0.0003	3	2	613.6099	-0.0028	29	28	668.6443	0.0001
26	27	551.3493	-0.0008	4	3	615.7150	-0.0014	30	29	670.7690	0.0006
25	26	553.3956	0.0014	5	4	617.8239	0.0023	31	30	672.8931	0.0005
24	25	555.4408	0.0002	6	5	619.9299	0.0017	32	31	675.0166	-0.0002
23	24	557.4911	0.0015	7	6	622.0400	0.0039	33	32	677.1405	-0.0004
22	23	559.5407	-0.0002	8	7	624.1456	0.0003	34	33	679.2646	-0.0003
21	22	561.5943	-0.0002	9	8	626.2565	0.0008	35	34	681.3891	0.0006
20	21	563.6507	0.0003	10	9	628.3672	-0.0001	36	35	683.5122	0.0002
19	20	565.7084	-0.0003	11	10	630.4790	-0.0010	37	36	685.6343	-0.0008
18	19	567.7695	0.0002	12	11	632.5941	0.0002	38	37	687.7572	-0.0006
17	18	569.8321	0.0001	13	12	634.7092	0.0005	39	38	689.8805	0.0005
15	16	573.9640	-0.0002	14	13	636.8244	-0.0001	40	39	692.0006	-0.0011
14	15	576.0327	-0.0009	15	14	638.9415	0.0002	41	40	694.1231	0.0003
13	14	578.1048	-0.0001	16	15	641.0582	-0.0008	42	41	696.2448	0.0017
12	13	580.1776	-0.0010	17	16	643.1766	-0.0009	43	42	698.3623	-0.0005
11	12	582.2542	0.0001	18	17	645.2968	0.0001	44	43	700.4821	0.0004
10	11	584.3327	0.0009	19	18	647.4169	0.0001				
9	10	586.4096	-0.0019	20	19	649.5378	0.0004				
						(01^10)—(000), f—e					
1	1	607.3188	-0.0026	17	17	609.0179	-0.0002	31	31	612.7993	0.0002
3	3	607.3812	0.0038	18	18	609.2185	0.0004	32	32	613.1489	0.0003
5	5	607.4743	-0.0040	19	19	609.4297	0.0006	33	33	613.5087	0.0003
6	6	607.5484	0.0030	20	20	609.6513	0.0003	34	34	613.8783	-0.0001
7	7	607.6221	-0.0016	21	21	609.8838	0.0001	35	35	614.2589	0.0002
8	8	607.7137	0.0004	22	22	610.1267	-0.0005	36	36	614.6490	-0.0001
9	9	607.8113	-0.0026	23	23	610.3821	0.0006	37	37	615.0491	-0.0006
10	10	607.9272	0.0015	24	24	610.6471	0.0005	38	38	615.4590	-0.0012
11	11	608.0486	0.0001	25	25	610.9223	0.0000	39	39	615.8815	0.0006
12	12	608.1830	0.0004	26	26	611.2090	0.0003	40	40	616.3110	-0.0004
13	13	608.3280	0.0004	27	27	611.5066	0.0009	41	41	616.7512	-0.0005
14	14	608.4831	-0.0006	28	28	611.8129	-0.0005	42	42	617.2012	-0.0007
15	15	608.6507	-0.0002	29	29	612.1319	0.0004	43	43	617.6604	-0.0014
16	16	608.8287	-0.0003	30	30	612.4608	0.0007	44	44	618.1331	0.0017
						(001)—(000)					
45	46	1541.0045	-0.0005	10	11	1624.0467	0.0002	24	23	1694.7873	-0.0008
44	45	1543.5319	0.0006	9	10	1626.2471	0.0001	25	24	1696.6107	-0.0002
43	44	1546.0486	-0.0005	8	9	1628.4375	0.0001	26	25	1698.4222	-0.0002
42	43	1548.5589	0.0005	7	8	1630.6155	-0.0022	27	26	1700.2221	-0.0002
41	42	1551.0588	-0.0002	6	7	1632.7857	-0.0021	28	27	1702.0115	0.0010
40	41	1553.5512	0.0003	4	5	1637.0972	-0.0001	29	28	1703.7878	0.0005
39	40	1556.0344	0.0004	3	4	1639.2396	0.0029	30	29	1705.5519	-0.0004
37	38	1560.9744	0.0005	2	3	1641.3651	-0.0005	31	30	1707.3056	-0.0001
36	37	1563.4317	0.0010	1	2	1643.4846	0.0003	32	31	1709.0471	-0.0002

Note. O–C denotes observed − calculated. Unless otherwise indicated, units are in cm^{-1}.

[a] Rotational-vibrational and pure rotational transitions weighted 1:10000.

[b] The observed transition frequencies labeled with asterisks were not included in the least-squares fit.

[c] Units in MHz.

TABLE 1—*Continued*

J'	J"	*Obs.*	O-C	J'	J"	*Obs.*	O-C	J'	J"	*Obs.*	O-C
35	36	1565.8787	0.0002	0	1	1645.5892	-0.0032	33	32	1710.7772	-0.0001
34	35	1568.3168	-0.0005					34	33	1712.4948	-0.0006
33	34	1570.7474	0.0002	2	1	1651.8551	0.0013	35	34	1714.2014	-0.0003
32	33	1573.1687	0.0008	3	2	1653.9221	0.0022	36	35	1715.8957	-0.0004
31	32	1575.5795	-0.0001	4	3	1655.9763	0.0011	37	36	1717.5784	-0.0003
30	31	1577.9821	0.0000	5	4	1658.0194	-0.0006	38	37	1719.2491	-0.0003
29	30	1580.3758	0.0003	6	5	1660.0542	0.0002	39	38	1720.9077	-0.0003
28	29	1582.7597	0.0001	7	6	1662.0771	-0.0001	40	39	1722.5541	-0.0005
27	28	1585.1341	-0.0004	8	7	1664.0898	0.0002	41	40	1724.1894	0.0002
26	27	1587.5002	0.0001	9	8	1666.0909	-0.0003	42	41	1725.8111	-0.0007
25	26	1589.8565	0.0002	10	9	1668.0825	0.0005	43	42	1727.4230	0.0008
24	25	1592.2030	-0.0001	11	10	1670.0616	-0.0001	44	43	1729.0208	0.0003
23	24	1594.5398	-0.0006	12	11	1672.0314	0.0008	45	44	1730.6068	0.0001
22	23	1596.8677	-0.0006	13	12	1673.9888	0.0003	46	45	1732.1793	-0.0013
21	22	1599.1866	0.0000	14	13	1675.9356	0.0004	47	46	1733.7418	-0.0005
20	21	1601.4956	0.0003	15	14	1677.8709	-0.0001	48	47	1735.2913	-0.0003
19	20	1603.7945	0.0000	16	15	1679.7960	0.0003	49	48	1736.8309	0.0022
18	19	1606.0843	0.0004	17	16	1681.7093	0.0001	50	49	1738.3522	-0.0013
17	18	1608.3635	-0.0002	18	17	1683.6108	-0.0006	52	51	1741.3667	0.0009
16	17	1610.6336	-0.0001	19	18	1685.5026	0.0000	53	52	1742.8543	0.0010
15	16	1612.8936	-0.0003	20	19	1687.3816	-0.0008	54	53	1744.3274	-0.0009
14	15	1615.1443	0.0000	21	20	1689.2505	-0.0003	56	55	1747.2396	-0.0013
13	14	1617.3849	0.0002	22	21	1691.1093	0.0013	58	57	1750.1058	0.0028
12	13	1619.6152	-0.0001	23	22	1692.9539	0.0002	59	58	1751.5134	-0.0017
11	12	1621.8360	0.0001								
						$(01^{1}1)$—$(01^{1}0)$, e—e					
48	49	1542.8486	0.0002	15	16	1620.3895	-0.0026	20	19	1695.2757	0.0001
47	48	1545.3562	0.0008	14	15	1622.5776	-0.0017	21	20	1697.2151	0.0000
46	47	1547.8521	-0.0009	13	14	1624.7611	0.0025	22	21	1699.1424	-0.0010
45	46	1550.3405	-0.0005	12	13	1626.9302	0.0000	23	22	1701.0608	0.0007
44	45	1552.8199	0.0006	11	12	1629.0940	-0.0003	24	23	1702.9654	0.0003
43	44	1555.2891	0.0011	10	11	1631.2515	0.0002	25	24	1704.8581	-0.0002
42	43	1557.7473	0.0002	9	10	1633.4005	-0.0010	26	25	1706.7395	0.0002
41	42	1560.1959	-0.0004	8	9	1635.5447	-0.0006	27	26	1708.6088	0.0004
40	41	1562.6367	0.0010	6	7	1639.8156	0.0002	28	27	1710.4680	0.0030
39	40	1565.0666	0.0013	5	6	1641.9433	0.0011	29	28	1712.3091	-0.0001
38	39	1567.4839	-0.0009	4	5	1644.0654	0.0015	30	29	1714.1401	-0.0007
37	38	1569.8945	-0.0001	3	4	1646.1810	0.0001	31	30	1715.9597	-0.0002
36	37	1572.2958	0.0015	1	2	1650.4000	-0.0011	33	32	1719.5587	-0.0012
35	36	1574.6844	0.0006					34	33	1721.3406	0.0000
34	35	1577.0632	-0.0003	2	1	1658.7883	-0.0010	35	34	1723.1090	0.0005
33	34	1579.4335	0.0004	3	2	1660.8736	-0.0015	36	35	1724.8646	0.0013
32	33	1581.7929	0.0003	4	3	1662.9524	-0.0036	37	36	1726.6022	-0.0028
31	32	1584.1356	-0.0064	5	4	1665.0339	0.0021	38	37	1728.3304	-0.0033
30	31	1586.4808	-0.0005	6	5	1667.1033	0.0013	40	39	1731.7519	0.0004
29	30	1588.8111	0.0005	8	7	1671.2247	0.0003	42	41	1735.1180	0.0015
28	29	1591.1318	0.0021	9	8	1673.2755	0.0000	43	42	1736.7721	-0.0070
27	28	1593.4383	-0.0005	10	9	1675.3190	-0.0006	44	43	1738.4283	0.0000
26	27	1595.7382	0.0002	11	10	1677.3565	0.0005	46	45	1741.6849	-0.0019
25	26	1598.0273	0.0002	12	11	1679.3841	-0.0003	47	46	1743.2952	-0.0008
23	24	1602.5739	-0.0019	13	12	1681.4054	0.0011	48	47	1744.8916	-0.0002
22	23	1604.8357	0.0002	14	13	1683.4155	0.0001	49	48	1746.4747	0.0006
21	22	1607.0856	0.0000	15	14	1685.4180	0.0007	50	49	1748.0387	-0.0043
20	21	1609.3253	-0.0008	16	15	1687.4083	-0.0011	51	50	1749.6003	0.0020
19	20	1611.5584	0.0011	17	16	1689.3903	-0.0014	52	51	1751.1421	0.0019
17	18	1615.9923	0.0001	18	17	1691.3624	-0.0012				
16	17	1618.1973	0.0009	19	18	1693.3257	0.0008				
						$(01^{1}1)$—$(01^{1}0)$, f—f					
47	48	1542.3783	0.0017	13	14	1624.1435	-0.0003	22	21	1698.2702	0.0006
46	47	1544.9242	-0.0021	12	13	1626.3847	-0.0005	23	22	1700.1277	0.0010
45	46	1547.4673	-0.0006	11	12	1628.6167	0.0000	24	23	1701.9708	-0.0016
44	45	1550.0007	-0.0005	10	11	1630.8387	0.0005	25	24	1703.8074	0.0007
43	44	1552.5257	-0.0004	9	10	1633.0497	0.0000	26	25	1705.6281	-0.0014
42	43	1555.0440	0.0014	8	9	1635.2512	0.0001	27	26	1707.4408	0.0001
40	41	1560.0507	0.0003	7	8	1637.4434	0.0010	28	27	1709.2409	0.0004
39	40	1562.5397	-0.0017	6	7	1639.6229	-0.0007	29	28	1711.0290	0.0003
38	39	1565.0220	-0.0018	5	6	1641.7943	-0.0003	30	29	1712.8050	-0.0001
37	38	1567.4963	-0.0014	4	5	1643.9560	0.0007	31	30	1714.5653*	-0.0047
36	37	1569.9622	-0.0007	2	3	1648.2471	0.0012	32	31	1716.3210	-0.0022
35	36	1572.4184	-0.0008	1	2	1650.3768	0.0011	33	32	1718.0655	0.0009
34	35	1574.8678	0.0012					34	33	1719.7937	-0.0007
33	34	1577.3051	-0.0003	3	2	1660.8736*	0.0063	35	34	1721.5138	0.0015
32	33	1579.7348	-0.0004	4	3	1662.9319	-0.0020	36	35	1723.2217	0.0033
31	32	1582.1571	0.0010	5	4	1664.9907	0.0008	37	36	1724.9130	0.0002
30	31	1584.5663	-0.0016	6	5	1667.0338	-0.0013	38	37	1726.6022*	0.0070
29	30	1586.9693	-0.0014	7	6	1669.0708	0.0012	39	38	1728.2650	-0.0007
28	29	1589.3654	0.0010	8	7	1671.0931	-0.0002	40	39	1729.9247	0.0005
27	28	1591.7483	-0.0007	9	8	1673.1061	0.0000	41	40	1731.5690	-0.0018
26	27	1594.1246	0.0004	10	9	1675.1082	0.0001	42	41	1733.2045	-0.0008
25	26	1596.4899	-0.0004	11	10	1677.0997	0.0005	43	42	1734.8278	0.0000
24	25	1598.8470	-0.0001	12	11	1679.0799	0.0005	44	43	1736.4405	0.0022
23	24	1601.1953	0.0008	13	12	1681.0476	-0.0008	45	44	1738.0368	0.0002
22	23	1603.5330	0.0004	14	13	1683.0070	0.0004	46	45	1739.6239	0.0010
21	22	1605.8610	-0.0001	15	14	1684.9537	0.0002	47	46	1741.1964	-0.0005
20	21	1608.1810	0.0008	16	15	1686.8889	-0.0006	48	47	1742.7606	0.0018
19	20	1610.4896	-0.0002	17	16	1688.8126	-0.0017	49	48	1744.3101	0.0016
18	19	1612.7886	-0.0010	18	17	1690.7278	-0.0001	51	50	1747.3742	0.0032
17	18	1615.0822	0.0022	19	18	1692.6277	-0.0026	52	51	1748.8808	-0.0031
16	17	1617.3606	0.0001	20	19	1694.5232	0.0019	53	52	1750.3828	-0.0016
15	16	1619.6315	0.0000	21	20	1696.4048	0.0037				

TABLE 1—*Continued*

J'	J"	*Obs.*	O-C	J'	J"	*Obs.*	O-C	J'	J"	*Obs.*	O-C
						(000)—(000)					
4	3	251535.4160[c]	0.0072	5	4	314410.0100[c]	0.0079	6	5	377278.4360[c]	0.0125
						(100)—(100)					
3	2	186422.6440[c]	-0.0745	6	5	372865.8520[c]	-0.0616				
						(001)—(001)					
4	3	250274.7810[c]	0.0376	5	4	312834.2250[c]	0.0222	6	5	375387.5730[c]	0.0615
						(01^11)—(01^11), e—e					
4	3	251725.7250[c]	0.0113	5	4	314647.7000[c]	-0.0164	6	5	377563.3880[c]	-0.0478
						(01^11)—(01^11), f—f					
4	3	252878.5750[c]	-0.0143	5	4	316088.6020[c]	0.0040	6	5	379292.1930[c]	0.0114

sumed to be 617 cm^{-1}, the matrix value reported by Lory and Porter (*15*). Table 4 lists the molecular constants thus obtained.

IV. DISCUSSION

The present study provided new data: the band origin of ν_1, the vibration–rotation constant α_1 for both $D^{11}BO$ and $D^{10}BO$, and the band origins of ν_2 and ν_3 of $D^{11}BO$, which were added to those already available to improve the equilibrium molecular structure and the harmonic and anharmonic force field of Ref. (*4*). It was found that the ν_1 frequency was poorly reproduced for the $H^{11}BO$, $H^{10}BO$, $D^{11}BO$, and $D^{10}BO$. This observation is ascribed to a large vibrational anharmonic constant x_{11} associated with the H(D)–B stretching mode, ν_1. In order to make corrections for this anharmonicity, the fundamental frequencies ν_1 of HBO and DBO were multiplied, respectively, by the ratios ω_1/ν_1 of HCN and DCN calculated from the data of Ref. (*16*) before the values were used for analysis. The input parameters are summarized in Table 5, and the equilibrium structure and force field which are derived are given in Table 6; in both of the tables the data reported in (*4*) are also included for comparison. The present results agree well with the previous ones, but, as expected, the harmonic and third-order anharmonic potential constants associated with the B–H stretching mode were much improved in precision.

As noted above, the $\nu_2 + \nu_3$ frequency obtained for $D^{11}BO$, 2262.96084 (81) cm^{-1}, slightly exceeds the sum of the two fundamental frequencies, ν_2 [608.36225 (53)] + ν_3 [1647.69007 (62)] = 2256.05232 (82) cm^{-1}; the x_{23} constant was calculated to be +6.909 cm^{-1}. It is interesting to note that the x_{23} constant is −3.38 and +2.73 cm^{-1} for HCN and DCN, respectively (*16, 17*). In the case of $D^{10}BO$,

TABLE 2
Molecular Constants of $D^{11}BO$[a,b]

Constant	Ground State	$v_1 = 1$	$v_2 = 1$	$v_3 = 1$	$v_2 = 1 + v_3 = 1$
ν		2253.52753 (65)	608.36225 (53)	1647.69007 (62)	2262.96084 (81)
B_v	1.0488445 (15)	1.039564 (18)	1.0520396 (14)	1.0435879 (17)	1.0467379 (89)
$10^6 D_v$	1.7159 (40)	1.7016 (80)	1.7666 (41)	1.7099 (38)	1.7567 (50)
$10^{12} H_v$	2.2 (13)	2.3 (18)	2.7 (14)	2.1 (12)	2.5 (14)
$10^3 q_v$			-4.8082 (18)		-4.910 (15)
$10^8 D_{qv}$			-3.94 (13)		-3.51 (32)
$\zeta^{\nu}_{1,2+3}$		0.07766 (23)			

[a] Values in parentheses denote three times the standard deviations, which apply to the last digits.
[b] Units are cm^{-1}, except $\zeta^{\nu}_{1,2+3}$, which is dimensionless.

TABLE 3

Rotational–Vibrational and Pure Rotational Line Positions for $D^{10}BO$[a,b]

J′	J″	Obs.	O-C	J′	J″	Obs.	O-C	J′	J″	Obs.	O-C
						(100)—(000)					
44	45	2194.5319	0.0148	12	13	2275.8901	0.0011	17	16	2338.9500	0.0000
43	44	2197.2076	0.0106	11	12	2278.2251	-0.0009	18	17	2340.7984	-0.0005
41	42	2202.5420	0.0006	0	11	2280.5442	-0.0035	19	18	2342.6335	0.0010
40	41	2205.2105*	0.0052	9	10	2282.8531	-0.0007	20	19	2344.4502	-0.0002
39	40	2207.8736*	0.0106	8	9	2285.1449	0.0008	21	20	2346.2546	0.0013
38	39	2210.5164	0.0022	7	8	2287.4187	-0.0001	22	21	2348.0394	-0.0017
37	38	2213.1652*	0.0067	6	7	2289.6751	-0.0022	23	22	2349.8130	-0.0011
36	37	2215.7984	0.0030	5	6	2291.9196	-0.0003	24	23	2351.5728	0.0004
35	36	2218.4249	0.0004	4	5	2294.1498	0.0036	25	24	2353.3165	0.0002
34	35	2221.0422	-0.0032	3	4	2296.3652*	0.0089	26	25	2355.0459	-0.0003
33	34	2223.6580	0.0002	2	3	2298.5591*	0.0091	27	26	2356.7598	-0.0022
32	33	2226.2618	0.0007	1	2	2300.7281	0.0009	28	27	2358.4618	-0.0024
31	32	2228.8537	-0.0013	0	1	2302.8846	-0.0034	29	28	2360.1538	0.0007
30	31	2231.4413	0.0022					30	29	2361.8270	-0.0018
29	30	2234.0183*	0.0053	1	0	2307.1623	0.0024	31	30	2363.4921	0.0004
28	29	2236.5755	-0.0009	2	1	2309.2608*	-0.0100	32	31	2365.1439	0.0017
27	28	2239.1284	-0.0004	3	2	2311.3644	-0.0008	33	32	2366.7797	-0.0006
26	27	2241.6596*	-0.0103	4	3	2313.4433	0.0004	34	33	2368.4077	0.0010
25	26	2244.1975	-0.0019	5	4	2315.5036	-0.0003	35	34	2370.0222	0.0008
24	25	2246.7160	-0.0009	6	5	2317.5503	0.0021	36	35	2371.6254	0.0005
23	24	2249.2226	0.0004	7	6	2319.5741	-0.0019	37	36	2373.2221	0.0046
22	23	2251.7160	0.0011	8	7	2321.5867	-0.0004	38	37	2374.8084	0.0089
21	22	2254.1961	0.0015	9	8	2323.5831	0.0014	40	39	2377.9458*	0.0127
20	21	2256.6614	0.0002	10	9	2325.5591	-0.0007	41	40	2379.4946*	0.0092
19	20	2259.1133	-0.0011	11	10	2327.5198	-0.0015	42	41	2381.0352*	0.0068
18	19	2261.5570	0.0032	12	11	2329.4670	0.0005	43	42	2382.5690*	0.0065
17	18	2263.9795	0.0002	13	12	2331.3966	0.0012	44	43	2384.0993*	0.0114
16	17	2266.3891	-0.0014	14	13	2333.3076	-0.0005	45	44	2385.6135*	0.0085
15	16	2268.7866	-0.0006	15	14	2335.2065	0.0019	47	46	2388.6265*	0.0112
14	15	2271.1719	0.0025	16	15	2337.0842	-0.0010	49	48	2391.6098*	0.0142
13	14	2273.5332	-0.0035								
						(001)—(000)					
49	50	1540.8794	-0.0003	17	18	1620.1571	-0.0002	14	13	1689.2273	-0.0007
46	47	1548.7027	-0.0019	16	17	1622.4775	-0.0005	15	14	1691.2057	-0.0003
45	46	1551.2966	0.0009	15	16	1624.7887	0	16	15	1693.1727	-0.0001
44	45	1553.8792	0.0010	14	15	1627.0887	-0.0007	17	16	1695.1312	0.0031
43	44	1556.4512	-0.0007	13	14	1629.3796	-0.0002	18	17	1697.0700	-0.0017
42	43	1559.0190	0.0021	12	13	1631.6601	-0.0001	19	18	1699.0045	0.0005
41	42	1561.5737	0.0006	11	12	1633.9302	-0.0002	20	19	1700.9242	-0.0004
40	41	1564.1189	-0.0016	10	11	1636.1979*	0.0076	21	20	1702.8323	-0.0014
39	40	1566.6573	-0.0016	9	10	1638.4411	0.0012	22	21	1704.7293	-0.0018
38	39	1569.1818*	-0.0066	8	9	1640.6798	0.0007	23	22	1706.6216	0.0048
37	38	1571.7124	0.0035	7	8	1642.9102	0.0021	24	23	1708.4888	-0.0020
36	37	1574.2209	0.0005	6	7	1645.1385*	0.0120	25	24	1710.3512	-0.0018
35	36	1576.7231	0.0003	5	6	1647.3369	0.0024	26	25	1712.2034	-0.0001
34	35	1579.2146	-0.0014	4	5	1649.5329	0.0009	28	27	1715.8670	-0.0017
33	34	1581.6977	-0.0024	3	4	1651.7198	0.0009	29	28	1717.6880	0.0045
32	33	1584.1734	-0.0014	2	3	1653.8944	-0.0008	30	29	1719.4907	0.0044
31	32	1586.6423	0.0020	0	1	1658.2167	0.0009	31	30	1721.2745	-0.0026
30	31	1589.0966	0					32	31	1723.0551	-0.0008
29	30	1591.5445	0.0010	1	0	1662.4988*	0.0054	33	32	1724.8211	-0.0015
28	29	1593.9851	0.0042	2	1	1664.6116	-0.0045	37	36	1731.7682	0.0003
27	28	1596.4095	0.0007	3	2	1666.7257	-0.0021	39	38	1735.1634	-0.0038
26	27	1598.8257	-0.0016	4	3	1668.8287	0.0001	40	39	1736.8518	0.0034
25	26	1601.2350	-0.0011	5	4	1670.9183	-0.0002	41	40	1738.5187	0.0016
24	25	1603.6350	-0.0004	6	5	1672.9883*	-0.0092	42	41	1740.1740	0.0005
23	24	1606.0247	-0.0002	7	6	1675.0661	0.0007	43	42	1741.8191	0.0017
22	23	1608.4033	-0.0016	8	7	1677.1182	-0.0040	45	44	1745.0680	0.0002
21	22	1610.7760	0.0010	9	8	1679.1676	-0.0003	46	45	1746.6762	0.0020
20	21	1613.1352	-0.0002	10	9	1681.2035	0.0012	47	46	1748.2634	-0.0046
19	20	1615.4862	0.0003	12	11	1685.2378	0.0000				
18	19	1617.8257	-0.0009	13	12	1687.2388	0.0002				
						(000)—(000)					
4	3	257116.0840[c]	0.2120	5	4	321385.4180[c]	0.2917	6	5	385648.2040[c]	0.2987
						(001)—(001)					
4	3	255823.1980[c]	-0.1606	5	4	319769.2650[c]	-0.2555	6	5	383708.8560[c]	-0.3750

Note. O–C denotes observed − calculated. Unless otherwise indicated, units are in cm^{-1}.

[a] Rotational-vibrational and pure rotational transitions weighted 1:10000.

[b] The observed transition frequencies labeled with asterisks were not included in the least-squares fit.

[c] Units in MHz.

where we neglected x_{23}, we obtained an effective Coriolis coupling constant that was about 30% larger than the value listed in Table 4.

The Coriolis interaction between the ν_1 and $\nu_2 + \nu_3$ states originates partly from mixing of the two vibrational states with others through anharmonic potential constants. Another source of the interaction arises from the first-order terms in the expansion of the B rotational constant in terms of the two stretching normal coordinates, which, when inserted in the two Coriolis interaction Hamiltonians, contribute directly to the interaction matrix element.

When we take into account only cubic anharmonic potential

TABLE 4
Molecular Constants of $D^{10}BO$[a,b]

Constant	Ground State	$v_1 = 1$	$v_3 = 1$	$v_2 = 1 + v_3 = 1$
ν		2305.0322 (13)	1660.3600 (10)	(2284.3)[c]
B_v	1.0721153 (23)	1.062343 (77)	1.0667259 (24)	(1.070240)[c]
$10^6 D_v$	1.8013 (31)	1.6437 (27)	1.7946 (32)	(1.801)[c]
$10^{12} H_v$	(2.2)[c]	(2.3)[c]	(2.1)[c]	(2.5)[c]
$10^3 q_v$		---	---	(-4.93271)[c]
$\zeta^y_{1,2+3}$	0.0833 (19)			

[a] Values in parentheses denote three times the standard deviations, which apply to the last digits.
[b] Units are cm^{-1}, except $\zeta^y_{1,2+3}$, which is dimensionless.
[c] Assumed.

terms $k_{ijk}q_iq_jq_k$, we may derive the following expression for the effective Coriolis interaction matrix element,

$$
\begin{aligned}
&[\langle 100|k_{113}|101\rangle + \langle 100|k_{333}|101\rangle + \langle 100|k_{223}|101\rangle] \\
&\quad \times \langle 101|C_1|011\rangle(-\tfrac{1}{2})[1/\omega_3 + 1/(\omega_1 - \omega_2)] \\
&\quad + \langle 100|k_{223}|121\rangle\langle 121|C_1|011\rangle(-\tfrac{1}{2})[1/(2\omega_2 + \omega_3) \\
&\quad + 1/(\omega_1 + \omega_2)] + \langle 100|C_1|010\rangle[\langle 010|k_{113}|011\rangle \\
&\quad + \langle 010|k_{333}|011\rangle + \langle 010|k_{223}|011\rangle](\tfrac{1}{2})[1/(\omega_1 - \omega_2) \\
&\quad + 1/\omega_3] + \langle 100|C_1|210\rangle\langle 210|k_{113}|011\rangle(-\tfrac{1}{2}) \\
&\quad \times [1/(\omega_1 + \omega_2) + 1/(2\omega_1 - \omega_3)] + \langle 100|k_{133}|002\rangle \\
&\quad \times \langle 002|C_3|011\rangle(-\tfrac{1}{2})[1/(2\omega_3 - \omega_1) + 1/(\omega_3 - \omega_2)] \\
&\quad + \langle 100|k_{122}|020\rangle\langle 020|C_3|011\rangle(-\tfrac{1}{2})[1/(2\omega_2 - \omega_1) \\
&\quad + 1/(\omega_2 - \omega_3)] + [\langle 100|k_{111}|000\rangle + \langle 100|k_{133}|000\rangle \\
&\quad + \langle 100|k_{122}|000\rangle]\langle 000|C_3|011\rangle(\tfrac{1}{2})[1/\omega_1 + 1/(\omega_2 + \omega_3)] \\
&\quad + \langle 100|C_3|111\rangle[\langle 111|k_{111}|011\rangle + \langle 111|k_{133}|011\rangle \\
&\quad + \langle 111|k_{122}|011\rangle](-\tfrac{1}{2})[1/(\omega_2 + \omega_3) + 1/\omega_1],
\end{aligned}
$$

where the cubic anharmonic terms $k_{ijk}q_iq_jq_k$ and the two Coriolis interaction terms ν_1/ν_2 and ν_3/ν_2 are symbolically expressed as k_{ijk} and C_i ($i = 1$ and 3), respectively. The effective Coriolis coupling constant from this source is thus equal to

$$
\begin{aligned}
&\zeta^{\text{eff}}_{st}[(\omega_t/\omega_s)^{1/2} + (\omega_s/\omega_t)^{1/2}](\mathrm{I}) \\
&\quad = \zeta_{12}/[2(2\omega_1\omega_2)^{1/2}] \times \{(k_{113} - k_{223})[(\omega_1 + \omega_2)/\omega_3 \\
&\quad + (\omega_1 + \omega_2)/(\omega_1 - \omega_2) - (\omega_1 - \omega_2)/(\omega_1 + \omega_2)] \\
&\quad - k_{113}(\omega_1 - \omega_2)/(2\omega_1 - \omega_3) \\
&\quad + k_{223}(\omega_1 - \omega_2)/(2\omega_2 + \omega_3)\} + \zeta_{32}/[2(2\omega_2\omega_3)^{1/2}] \\
&\quad \times \{(k_{133} + k_{122})[-(\omega_3 - \omega_2)/\omega_1 \\
&\quad - (\omega_3 - \omega_2)/(\omega_3 + \omega_2) + (\omega_3 + \omega_2)/(\omega_3 - \omega_2)] \\
&\quad + k_{133}(\omega_3 + \omega_2)/(2\omega_3 - \omega_1) \\
&\quad + k_{122}(\omega_3 + \omega_2)/(\omega_1 - 2\omega_2)\}.
\end{aligned}
$$

When the Coriolis resonance is exact, we may insert the relation $\omega_1 = \omega_2 + \omega_3$ in the above formula to simplify the result as follows:

$$
\begin{aligned}
&\zeta^{\text{eff}}_{st}[(\omega_t/\omega_s)^{1/2} + (\omega_s/\omega_t)^{1/2}](\mathrm{I}) \\
&\quad = 2(2)^{1/2}\{\zeta_{12}[(\omega_1\omega_2)^{1/2}/(\omega_1^2 - \omega_2^2)](k_{113} - k_{223}) \\
&\qquad + \zeta_{32}[(\omega_2\omega_3)^{1/2}/(\omega_3^2 - \omega_2^2)](k_{122} + k_{133})\}.
\end{aligned}
$$

The second part may be derived in the following way. The B rotational constant may be expanded in terms of the two stretching normal coordinates as follows,

$$B = B_e - B_e \sum_s (2B_e/\omega_s)^{1/2} 2c\zeta_{s2} q_s + \cdots,$$

where $s = 1$ or 3 and $c = +1$ and -1 for the two modes, respectively. These first-order terms, when inserted in the

TABLE 5
Input Parameters for the Determination of the Force Field of HBO

parameter[a]	obs	weight	This work obs - calc	Ref. (4) obs - calc
$H^{11}BO$				
B_0	39224.247	10000	-0.015	-0.085
ω_1	2903.6	100	0.5	[2820.76]
ω_2	754.4152	1000	-0.2932	0.0985
ω_3	1825.5561	1000	-0.2056	0.0578
α_1	269.785	200	-0.755	0.758
α_2	-86.255	200	-0.128	-0.015
α_3	259.249	200	-0.217	0.058
q_2	-181.925	100	-3.458	-0.714
D_0	80.24	20	-0.45	-0.36
$H^{10}BO$				
B_0	40575.395	10000	-0.241	-0.121
ω_1	2928.1	100	-0.2	[2844.47]
ω_2	763.6257	1000	-0.4704	-0.0707
ω_3	1864.1620	1000	0.2479	-0.59
α_1	299.502	200	-0.904	-0.865
α_2	-98.302	200	-0.184	-0.142
α_3	268.671	200	-0.832	-0.252
q_2	-192.388	100	-3.785	-0.883
D_0	85.75	20	-0.21	-0.10
$D^{11}BO$				
B_0	31443.572	10000	0.114	0.092
ω_1	2316.1	100	0.4	7.3[b]
ω_2	608.3623	1000	1.2582	-0.7
ω_3	1647.6901	1000	-0.2286	1.5
α_1	278.234	200	4.382	-1.901
α_2	-95.786	200	-0.302	0.634
α_3	157.589	200	0.492	0.449
q_2	-144.147	100	-1.874	0.371
D_0	51.44	20	0.25	0.24
$D^{10}BO$				
B_0	32141.214	10000	-0.069	-0.070
ω_1	2369.0	100	0.6	-1.2[b]
ω_2	617	1	-1.7	-1.4
ω_3	1660.3600	1000	0.1094	5.1[b]
α_1	292.956	200	-2.688	1.983[c]
α_2	-105.349	200	-0.194	-0.745
α_3	161.572	200	0.435	-0.353
q_2	-147.879	100	-1.989	0.315
D_0	54.00	20	0.31	0.32
$H^{11}B^{18}O$				
B_0	37529.818	10000	0.211	0.101
D_0	73.89	20	-0.15	-0.12
$H^{10}B^{18}O$				
B_0	38913.622	10000	0.026	0.098
D_0	79.17	20	0.23	0.27

[a] Units are cm^{-1} for ω_i, MHz for α_i and q_2, kHz for D_0.
[b] Weight is 1 in the least squares analysis.
[c] Not included in the least squares fitting.

TABLE 6
Equilibrium Structures and Force Fields of HBO[a]

parameter[b]	This study	Ref. (4)
r_e(B-H) / Å	1.16740 (74)	1.16667 (41)
r_e(B=O) / Å	1.20051 (20)	1.20068 (10)
f_{rr} / aJÅ^{-2}	4.377 (14)	4.169 (97)
f_{rR} / aJÅ^{-2}	-0.129 (18)	0.052 (90)
f_{RR} / aJÅ^{-2}	14.118 (38)	13.986 (103)
$f_{\alpha\alpha}$ / aJ	0.3256 (12)	0.3249 (5)
f_{rrr} / aJÅ^{-3}	-21.02 (29)	-20.92 (125)
f_{rrR} / aJÅ^{-3}	0.05 (29)	-0.147 (122)
f_{rRR} / aJÅ^{-3}	(0.0)	(0.0)
f_{RRR} / aJÅ^{-3}	-88.97 (91)	-88.39 (93)
$f_{r\alpha\alpha}$ / aJÅ^{-1}	-0.05 (16)	-0.046 (52)
$f_{R\alpha\alpha}$ / aJÅ^{-1}	-0.39 (14)	-0.381 (44)

[a] Values in parentheses denote three times the standard deviations, which apply to the last digits.
[b] The suffixes *r* and *R* denote the H—B and B═O bonds, respectively.

ordinary Coriolis interaction terms C_i in place of B, add the following to the effective Coriolis coupling constant:

$$\zeta_{st}^{\mathrm{eff}}[(\omega_t/\omega_s)^{1/2} + (\omega_s/\omega_t)^{1/2}](\mathrm{II}) = -2B_e^{1/2}[\zeta_{32}^2(\omega_3 - \omega_2) + \zeta_{12}^2(\omega_1 + \omega_2)]/(\omega_1\omega_2\omega_3)^{1/2}.$$

The cubic potential constants and the Coriolis coupling constants ζ_{12} and ζ_{32} were calculated from the force field listed in Table 6 and were inserted, together with the observed fundamental frequencies in place of the harmonic frequencies, in the above expressions to derive the effective Coriolis coupling constants, 0.0891 and 0.0916 for $D^{11}BO$ and $D^{10}BO$, respectively, which favorably compare with the observed values 0.07766 (*23*) and 0.0833 (*19*), respectively.

ACKNOWLEDGMENTS

We are grateful to Toshinori Suzuki, Kentarou Kawaguchi, and Masaharu Fujitake for help in observing the infrared diode laser and microwave spectra of DBO at the Institute for Molecular Science. The present work was supported

by the Joint Studies Program of the Institute for Molecular Science. Funding was also provided by the Natural Sciences and Engineering Research Council of Canada.

REFERENCES

1. E. F. Pearson and R. V. McCormick, *J. Chem. Phys.* **58,** 1619–1621 (1973).
2. Y. Kawashima, K. Kawaguchi, and E. Hirota, *Chem. Phys. Lett.* **131,** 205–208 (1986).
3. Y. Kawashima, Y. Endo, K. Kawaguchi, and E. Hirota, *Chem. Phys. Lett.* **135,** 441–445 (1987).
4. Y. Kawashima, Y. Endo, and E. Hirota, *J. Mol. Spectrosc.* **133,** 116–127 (1989).
5. P. Colarusso and P. Bernath, 51st International Symposium on Molecular Spectroscopy, Paper MG01, Columbus, OH, 1996.
6. E. Hirota, *in* ''Chemical and Biochemical Applications of Lasers'' (C. B. Moore, Ed.), Vol. V, pp. 39–93, Academic Press, New York, 1980.
7. E. Hirota, ''High-Resolution Spectroscopy of Transient Molecules,'' Springer, Heidelberg, 1985.
8. G. Guelachvili and K. Narahari Rao, ''Handbook of Infrared Standards,'' Academic Press, Orlando, 1986.
9. Frequency table prepared by Y. Hamada and supplied to us by his courtesy.
10. Y. Endo, S. Saito, and E. Hirota, *J. Chem. Phys.* **75,** 4379–4384 (1981).
11. Y. Endo and E. Hirota, *J. Chem. Phys.* **86,** 4319–4326 (1987).
12. P. Colarusso, K. Q. Zhang, and P. F. Bernath, in preparation.
13. C. P. Rinsland, M. A. H. Smith, A. Goldman, V. M. Devi, and D. C. Brenner, *J. Mol. Spectrosc.* **159,** 274–278 (1993).
14. H. G. Hedderich, K. Walker, and P. F. Bernath, *J. Mol. Spectrosc.* **149,** 314–316 (1991).
15. E. R. Lory and R. F. Porter, *J. Amer. Chem. Soc.* **93,** 6301–6302 (1971).
16. G. Strey and I. M. Mills, *Mol. Phys.* **26,** 129–138 (1973).
17. A. Maki, W. Quapp, S. Klee, G. C. Mellau, and S. Albert, *J. Mol. Spectrosc.* **180,** 323–336 (1996).